PFC/JA-87-26

A Pseudo-Tomographic Fitting Algorithm for Density Profile Reconstruction from a Sparse 1-D Interferometer Array

J.A. Casey, E. Sevillano, J.H. Irby, and B.G. Lane.

December 1987

Plasma Fusion Center
Massachusetts Institute of Technology
Cambridge, Massachusetts 02139 USA

This work was supported by the Department of Energy under contract number DE-AC02-78ET51013. Reproduction, translation, publication, use and disposal, in whole or part, by or for the United States government is permitted.

Submitted for publication in: *Review of Scientific Instruments*

Abstract

An algorithm has been developed for "real-time" analysis of a sparse multi-chord interferometer array, yielding peak density, Gaussian width, radial offset, ellipticity, and instability amplitude and frequency from line integrated density measurements. An automated analysis job produces processed data showing the evolution of profile parameters between shots on the Tara tandem mirror experiment. An assumption of plasma rigidity is necessary to trade temporal resolution (on instability timescales) for spatial resolution across the moving plasma column; the relevance of this assumption for Tara is discussed.

I Introduction

Detailed analysis of equilibrium and stability parameters in plasma fusion experiments requires diagnostics of the radial plasma density profile. Interferometry provides line-integrated density measurements. Reconstruction of multi-channel interferometry (sampled across several chords) can yield a spatial density profile. This requires either sufficient density of channels in two dimensions for tomographic reconstruction (usually using maximum entropy methods), or an assumption of azimuthal symmetry and a dense one dimensional array for Abel inversion.

We describe here a compromise algorithm for two-dimensional analysis of a density profile from a sparse (3-6 channel) one dimensional array of interferometers. The assumption of azimuthal symmetry has been relaxed, but an assumption of plasma column rigidity has been imposed. We compare all interferometer channels during a window a few MHD oscillations long ($\approx$ 1 msec) to expected signals generated from a simple model. The coefficients of the model are iteratively optimized using the *Levenberg-Marquardt method* of non-linear least-squares. One disadvantage of this method of course, is that fail-

ure of the "rigidity" assumption causes failure of the model and of the calculation. In effect, we assume a low order Fourier space perturbation of the plasma, thus higher order Fourier space fluctuations or spatially localized fluctuations will not be resolved, as they can be in larger arrays[1-3]. In addition, since we are relying on moderately large (greater than 2 cm) perturbations to provide a "spatial sweep" of the interferometer chords across the plasma frame of reference, very stable plasmas fail to provide sufficient resolution for high confidence fits, and the result becomes identical to a single time point simple Gaussian profile fit.

By taking advantage of the symmetry of the unstable modes of the plasma, we can extract details of the plasma evolution with a simple calculation that can be performed in "real time" (i.e. in the 5-10 minute interval between shots) without adding a substantial computational burden to the existing facilities. By choosing a suitable model for the plasma fluctuations, parameters describing the density profile and fluctuation trajectory are automatically optimized, and time-intensive inspection and cross-correlations[4,5] are avoided. This calculation has proved sufficiently robust to run in unattended batch jobs, and has been added to the standard analysis set of the Tara experiment.

II Hardware

Tara is a tandem mirror with axisymmetric plugs and outboard minimum-B anchors[6], see figure 1. The central cell plasma is typically

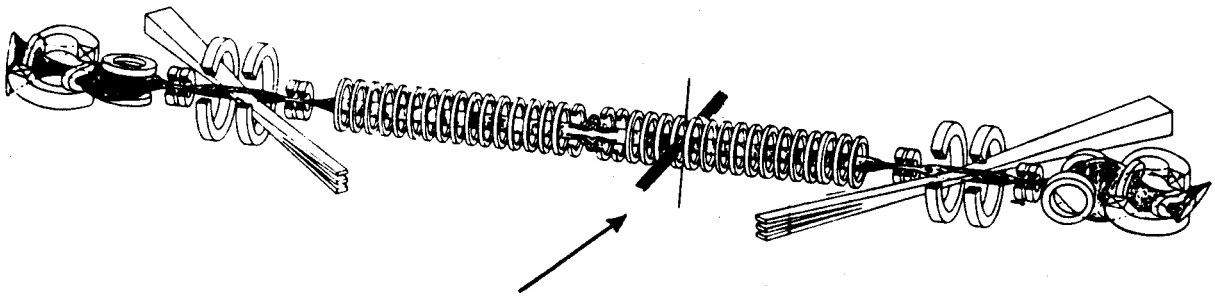

Figure 1. The Tara magnetic coil set, flux tube, and neutral beamlines are shown. The experiment is about 20 m end to end. The multi-chord interferometer array diagnostic (5 horizontal chords and 1 vertical chord) in the central cell is shown highlighted.

$2 - 5 \times 10^{12}$ cm^{-3} peak density, with a limiter radius of 19 cm. An array of 11 parallel horizontal interferometer feedthroughs was installed in the central cell at one axial location – currently we are operating 5 channels in the array. In addition, a vertical interferometer has been added at the same axial location[7].

The array consists of 6 self-contained interferometers which use frequency swept microwave sources as the basis of the operation of the system. They are commonly referred to as serrodyne, or in the older

literature as "zebra" pattern interferometers. The microwave sources used are 60 GHz Gunn oscillators with typical power output of 50 mW which are swept with a sawtooth of frequency $f_{\rm swp} = 1$ MHz. The source is connected to a ferrite isolator housed inside a soft iron tube used to shield the magnetic fields during the plasma discharges. The isolator, which prevents reflections back to the source, is followed by a 10 dB side-arm coupler which splits the power into the two interferometer arms. The detector is a double balanced mixer, a device whose intermediate frequency (IF) output has two different frequency components given by the sum and difference of the input frequencies at the local oscillator (LO), which comes from the reference leg, and the signal (RF) input, which traverses the plasma. The phase shift introduced by the plasma $\Delta\phi(t)$, which can be related to the line integral of the electron density, is contained in the difference frequency signal of the IF output of the mixer. This term is proportional to $\cos(k_g(t)\Delta L - \Delta\phi(t))$, where $k_g = 2\pi/\lambda_g$ and ΔL is an additional length of waveguide purposely introduced in one of the legs of the interferometer.

The time dependence of k_g is a consequence of the frequency sweep since the wavenumber for the dominant mode in the waveguide is fre-

quency dependent and is given by:

$$k_g = 2\pi[(\frac{f_o}{c})^2 - (\frac{1}{2a})^2]^{1/2} \tag{1}$$

where c is the speed of light and a the major dimension of rectangular waveguide. For times less than a ramp period, the guide wave number is given by:

$$k_g(t) = k_g(0) + \frac{\Delta k_g}{2\pi}\Omega t = k_g(0) + \frac{1}{2\pi}\frac{dk_g}{df_o}\Delta f_o \Omega t \tag{2}$$

where Δf_o is the amount the source frequency is swept and $\Omega = 2\pi f_{\mathrm{swp}}$. Substituting for this value of k_g, the IF output has the form $\cos(n\Omega t - \Delta\phi + \phi_o)$, where n is given by

$$n = \frac{1}{2\pi}\frac{dk_g}{df_o}\Delta f_o \Delta L = \frac{\Delta L}{\lambda_g}(\frac{\lambda_g}{\lambda_o})^2\frac{\Delta f_o}{f_o}. \tag{3}$$

The interferometer is adjusted to obtain integer values of n, usually $n = 1$ or one complete cycle. In this case the IF output is modulated at the sweep frequency.

Finally, the IF output from mixer is pre-amplified and sent to a phase detection system. The phase between a reference square wave from the ramp generator is compared to the square wave of the IF output that results from a bandpass filter and limiting amplifier. The phase sensitivity is $2\pi/16$ limited by the internal clock of the phase detection module which runs at 16 MHz.

III Fitting Algorithm

The key assumption for this analysis is that the plasma column is rigid, i.e. evolution in the shape of the plasma column takes place over timescales significantly longer than a rotation period. This allows the sparse one-dimensional array of interferometer chords to rotate around the plasma column in the frame of reference of the plasma. We thus exchange time resolution for spatial resolution. In a few rotation periods, many (several hundred) data points are gathered from the array. Given the rotation parameters of the plasma column, each data point becomes a chordal measurement parameterized by azimuthal angle and impact parameter. In fact, the real time analysis algorithm simultaneously optimizes the parameters characterizing the rotation and the shape of the plasma column. The accuracy of the results are therefore limited by the accuracy of the assumption of rigidity, and by the slowness with which the profile parameters evolve.

In general, the number of parameters describing this motion will exceed the number of data channels. There are two classes of solutions to this problem. First, if the amplitude of coherent oscillation is zero or very small, the number of data points is reduced from (# channels $\times$

time-points) to (# channels). In this case, the time resolution of the data plays no role – the data is averaged, and the amplitude, frequency, and phase of the oscillating motion become neutral parameters in the fit. The remaining parameters (which now must number fewer than the number of data channels) are fit to a constant profile. Of more interest is the case where the amplitude of coherent oscillation is non-negligible. In this case, the individual data channels sweep out paths of varying impact parameter and azimuth during the oscillation, and the resolution improves accordingly.

The coherent mode analysis uses an iterative non-linear least squares fitting routine, MRQMIN[8], which minimizes the χ^2 residual for a user supplied function of N parameters by optimizing the parameter values. We supply a function which calculates the line integrated density of an offset chord assuming a given profile model. The model used is a Gaussian profile with ellipticity, offset, and a continuous rotation around the offset axis:

$$n_e(\mathbf{r}) = n_e \exp\left(- \frac{x'^2 + \epsilon y'^2}{r_0^2} \right), \qquad (4)$$

with x' and y' co-rotating with the plasma column:

$$x' = x\ \cos\theta + y\ \sin\theta$$

$$y' = y\ \cos\theta - x\ \sin\theta$$

$$\theta = \omega t + \delta.$$

Expanding in the fixed (lab) coordinates yields

$$n_e = n_0\ \exp\left(-\frac{1}{r_0^2}\ \left(\alpha x^2 + \beta xy + \gamma y^2\right)\right) \tag{5}$$

for

$$\alpha \equiv\ \cos^2\theta + \epsilon\ \sin^2\theta$$

$$\beta \equiv (1-\epsilon)\ \sin(2\theta)$$

$$\gamma \equiv\ \sin^2\theta + \epsilon\ \cos^2\theta,$$

which can be integrated along the interferometer path giving

$$\begin{aligned} n_l &= \int_{-\infty}^{+\infty} dx\, n_0\ \exp\left(-\frac{1}{r_0^2}\ \left(\alpha x^2 + \beta xy + \gamma y^2\right)\right) \\ &= \sqrt{\frac{\pi}{\alpha}}\, n_0\, r_0\ \exp\left(-\frac{\epsilon a^2}{\alpha r_0^2}\right); \end{aligned} \tag{6}$$

for

$$a \equiv a_0 - b_0 - b_1\cos\theta, \tag{7}$$

where a_0 is the vertical offset of the interferometer, b_0 is the vertical offset of the plasma rotation center, and b_1 is the oscillation amplitude. Similarly, for a vertical interferometer,

$$n_l = \sqrt{\frac{\pi}{\gamma}}\, n_0\, r_0\ \exp\left(-\frac{\epsilon a'^2}{\gamma r_0^2}\right); \tag{8}$$

for

$$a' \equiv a'_0 - b'_0 + b_1 \sin\theta, \tag{9}$$

where a'_0 is the horizontal offset of the interferometer, and b'_0 is the horizontal offset of the plasma rotation center.

For fixed rather than co-rotating ellipticity, a similar calculation yields

$$\begin{aligned} n_{l\,\mathrm{horiz}} &= \sqrt{\pi}\, n_0\, r_0\, \exp\left(-\frac{\epsilon' a^2}{r_0^2}\right) \\ n_{l\,\mathrm{vert}} &= \sqrt{\frac{\pi}{\epsilon'}}\, n_0\, r_0\, \exp\left(-\frac{a'^2}{r_0^2}\right). \end{aligned} \tag{10}$$

Comparisons of χ^2 values generated from fits with fixed and co-rotating ellipticity generally show better fits with co-rotating ellipticity in our experiments. Our analysis program generalized equations (6), (8), and (10) to calculate line densities with both ϵ and ϵ' specified, but was always run with one or both parameters held fixed at a value of 1 (circular).

Typically, the least-squares fit optimizes the seven paramters: n_e (peak density), r_0 (1/e width), ϵ (ellipticity), b_0 (fixed offset normal to the interferometer line-of-sight), b_1 (amplitude of oscillation), ω (frequency of oscillation), and δ (phase of oscillation). Figure 2 models the density profile with typical values of these parameters.

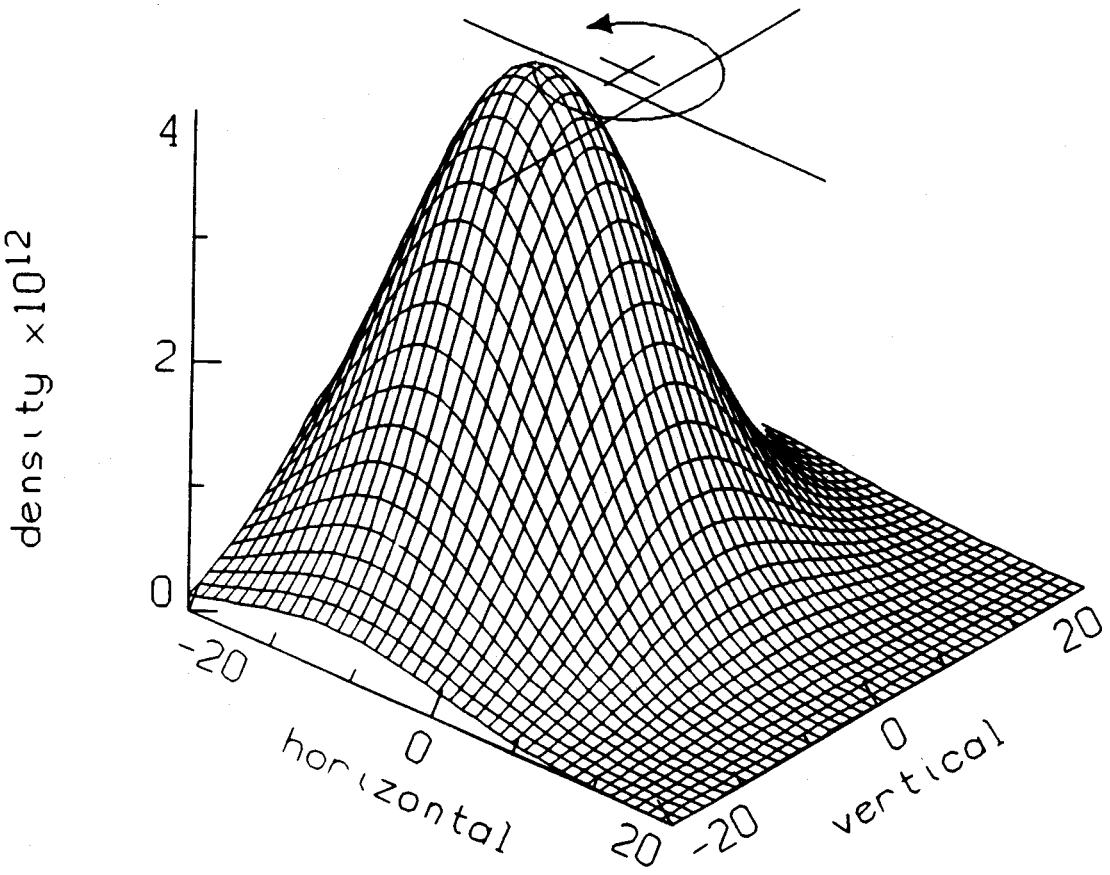

Figure 2. The two dimensional density profile model is shown for parameters $n_e = 4 \times 10^{12}\,\mathrm{cm}^{-3}$, $r_0 = 12\,\mathrm{cm}$, $\epsilon = 1$, $b_0 = 2\,\mathrm{cm}$, $b_0' = -3\,\mathrm{cm}$, and $b_1 = 6\,\mathrm{cm}$. The offset center of rotation and the rotation path are shown. This shot is shown with no ellipticity ($\epsilon = 1$); slight azimuthal elongation ($\epsilon \approx 1.1 - -1.5$) is not uncommon at larger rotation amplitudes.

The two parameter nature of the fit (time and chord offset) is eliminated by stacking the data from all chords onto the same time base. Each data point represents a measurement of the line density from an impact parameter in the plasma frame of reference that is not only de-

pendent on the chord offset, but also on the profile offset and instability amplitude and phase. In effect, the two input parameters transform into a single normalized parameter (a or a', see equations (7)and (9)), with the transformation coefficients determined by the density profile offset and the amplitude and phase of rotation. Since simple fitting algorithms require a single independent variable, we "hide" the fixed chord offsets by parameterizing all data by time, and adding large time offsets to different chord radii. The line-density model routine decodes the time base offsets to properly offset the interferometer chords via hidden common variables. A large ΔT is required between chords to insure that the phase of the oscillation is not perturbed by this method,

$$\frac{\tau}{\Delta T} \ll \frac{\delta t}{\tau}, \tag{11}$$

where τ is the period of oscillation, and δt is the resulting phase error induced by projecting all chords onto one time base. With a 50 kHz sampling rate assumed to reflect the allowable phase error, and a 10 kHz typical rotation period, 1 second is sufficient for ΔT.

We unfortunately have found that local minima of χ^2 can be found at harmonics and subharmonics of the rotation frequency. However, a pre-analysis FFT of each time window yields the frequency of peak

power, which is used as an initial guess in the iterative fit to improve performance.

Our analysis of the interferometer data generally fits a 1 msec window (50 time points $\times$ 4-5 interferometer channels) to our model, generating one value of each of the above parameters for each 1 msec window in the shot. The width of the window must be large enough to include several rotations, yet be small enough so that coherence is generally maintained within the window. Our application allows any of the adjustable parameters to be fixed at a given value to reduce the number of degrees of freedom and improve the fit, (i.e. to re-analyze a shot where the plasma profile appears circular, the ellipticity variable may be turned off). This method has the advantage of being automated; and the histogrammed data is processed and displayed in real-time during a run.

IV Plasma Rigidity and Mode Structure

The rotation of the density profile around the machine axis is caused by the $\mathbf{E} \times \mathbf{B}$ drifting of the plasma in a positive potential. A

positive potential is maintained in a simple mirror because of the greater loss rate of electrons into the velocity space loss cone. In a tandem mirror this ambipolar potential can be enhanced by plugging potential formation, direct electron heating, and endwall biasing. Both electrons and ions $\mathbf{E} \times \mathbf{B}$ drift across field lines at the same velocity to lowest order, but quasi-neutrality must also be preserved at higher order in bulk motions of the plasma. Finite ion Larmour radius (FLR) effects, field line curvature, and ion polarization drifts provide sources of net charge at higher order. For non-rigid MHD modes, FLR dominates and stabilizes small perturbations[9,10].

In Tara, $m > 1$ modes are generally stabilized by FLR, and the $m = 1$ mode typically saturates at finite amplitude rather than growing until the plasma is lost to the chamber walls. The characterization of the $m = 1$ mode has been studied extensively elsewhere[11,12].

V Results

Figure 3 shows the fast timescale accuracy of the fitting analysis. An analysis window 1.4 msec long yields results with a high statistical

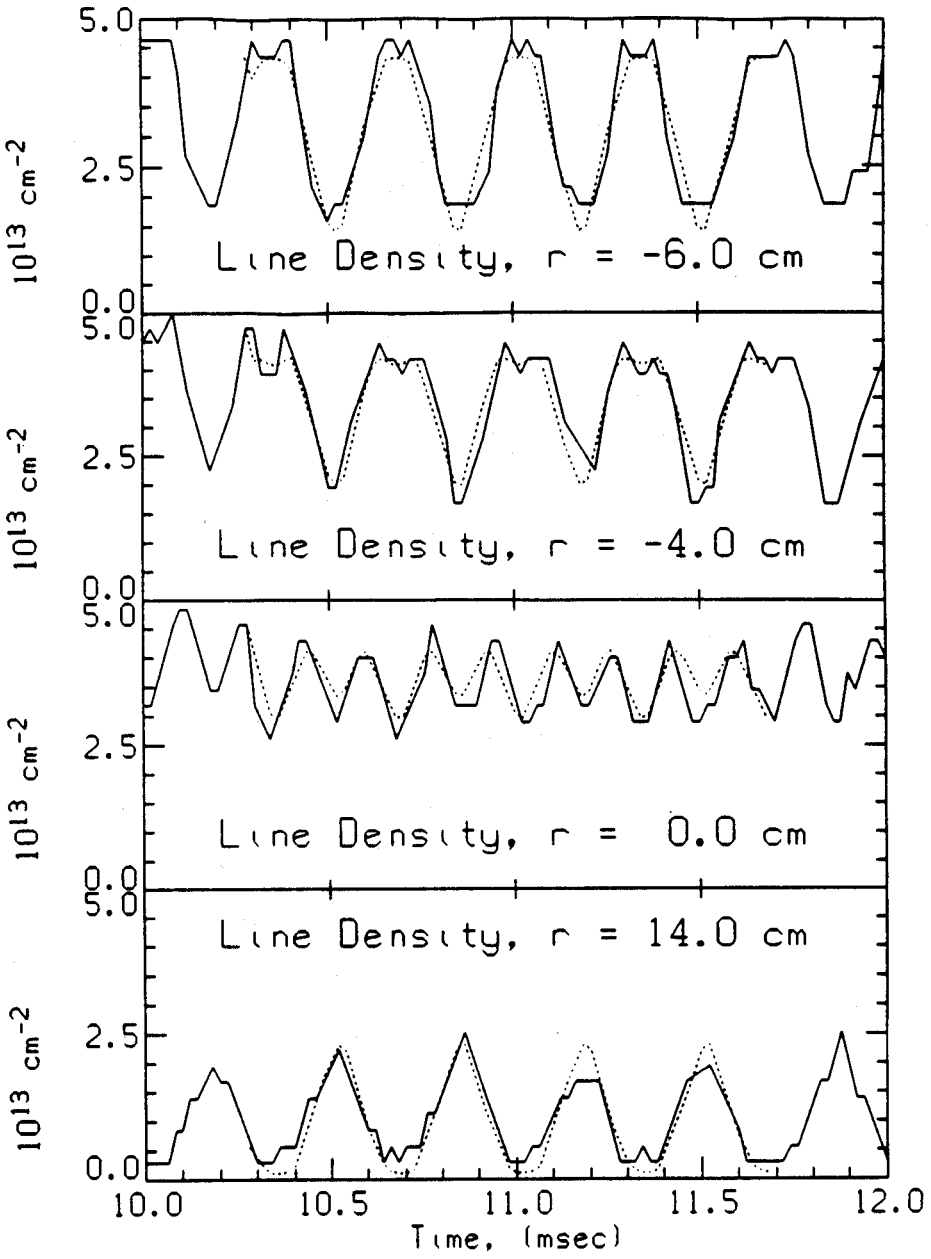

Figure 3. The raw line-density data from four horizontal chords is shown above in expanded time resolution. For the period from 10.3 msec to 11.7 msec, our analysis shows parameters of $n_e = 2.15 \times 10^{12}\,\mathrm{cm}^{-3}$, $r_e = 11.4\,\mathrm{cm}$, $b_0 = -0.6\,\mathrm{cm}$, $\epsilon = 1.12$, and rotation amplitude $b_1 = 6.1\,\mathrm{cm}$ and frequency $\omega/2\pi = 3.0\,\mathrm{kHz}$. Reconstructing the raw data from this analysis yields the dotted curves.

confidence level. In addition, reconstructing the raw data from the output parameters (including the phase) reproduces the raw data quite well (dotted curves). Note that the center chord shows a strong harmonic component due to the peak density passing through twice every cycle. The same phenomena produces a dimple in the line density peaks on the -4 cm chord. These features are reproduced quite well by the model.

Over longer timescales, the slow evolution of the profile parameters can be seen. Figure 4 shows that an $m = 1$ instability is excited by ECRH (electron cyclotron resonant heating) in one of the "plug" cells. The interferometer analysis shows three stages in the instability evolution. Before the start of heating the plasma is quiescent. After heating starts a small (2 cm) amplitude, 9 kHz oscillation begins. 15 msec later stability is lost and the amplitude of the oscillation grows to 7-8 cm while the frequency drops to 5 kHz. The last stage of this process shows a marked drop in peak density and average raw line density.

Another phenomena seen over long timescales is the profile evolution during axial "plugging". In figure 5, the peak density rises immediately after application of ICRF (ion cyclotron range of frequencies)

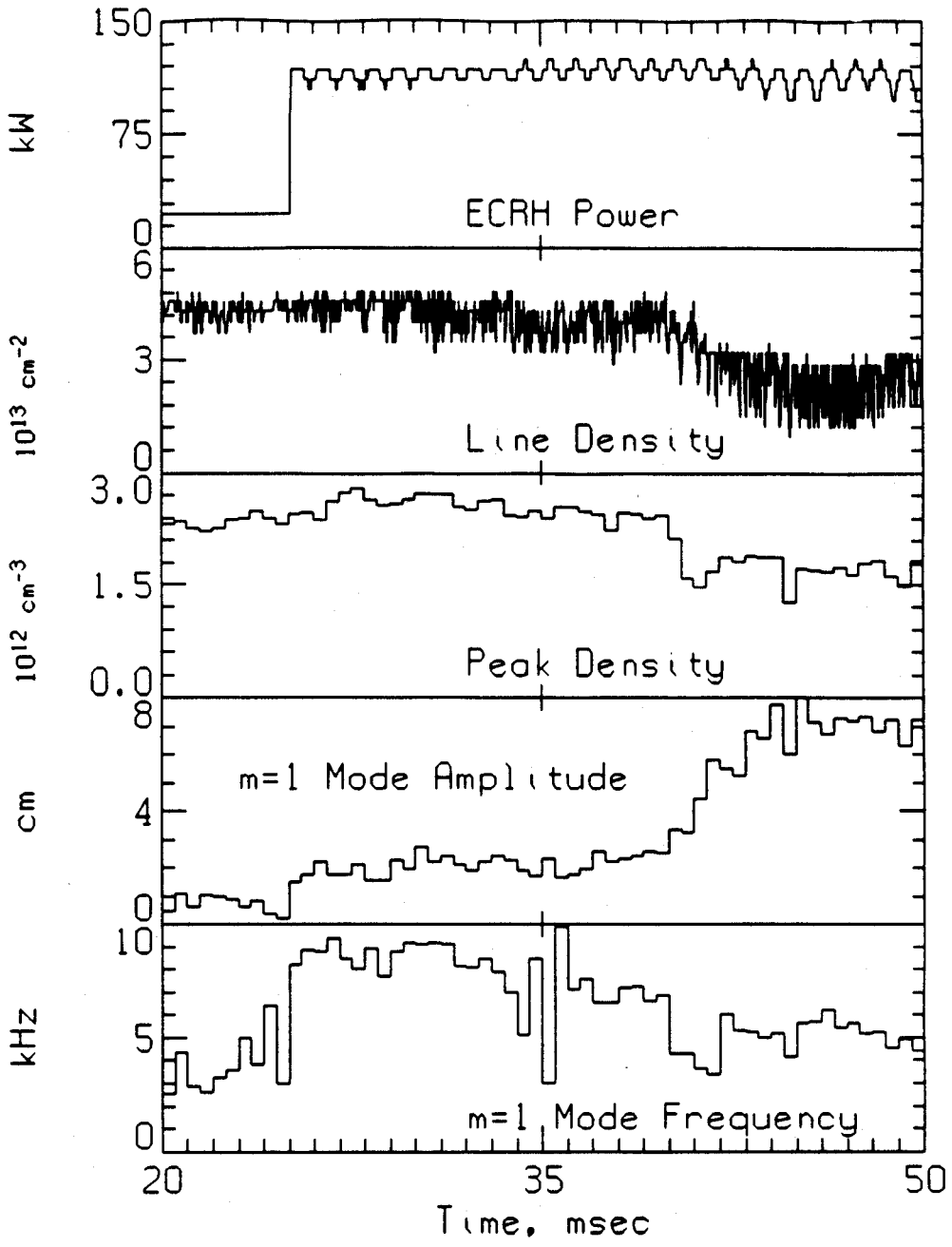

Figure 4. The frequency and amplitude of the MHD rotation are shown during application of ECRII (electron cyclotron resonant heating). Note the increased amplitude of rotation immediately after the heating turns on while stability is maintained, and the larger amplitude rotation during the "dump" of the plasma.

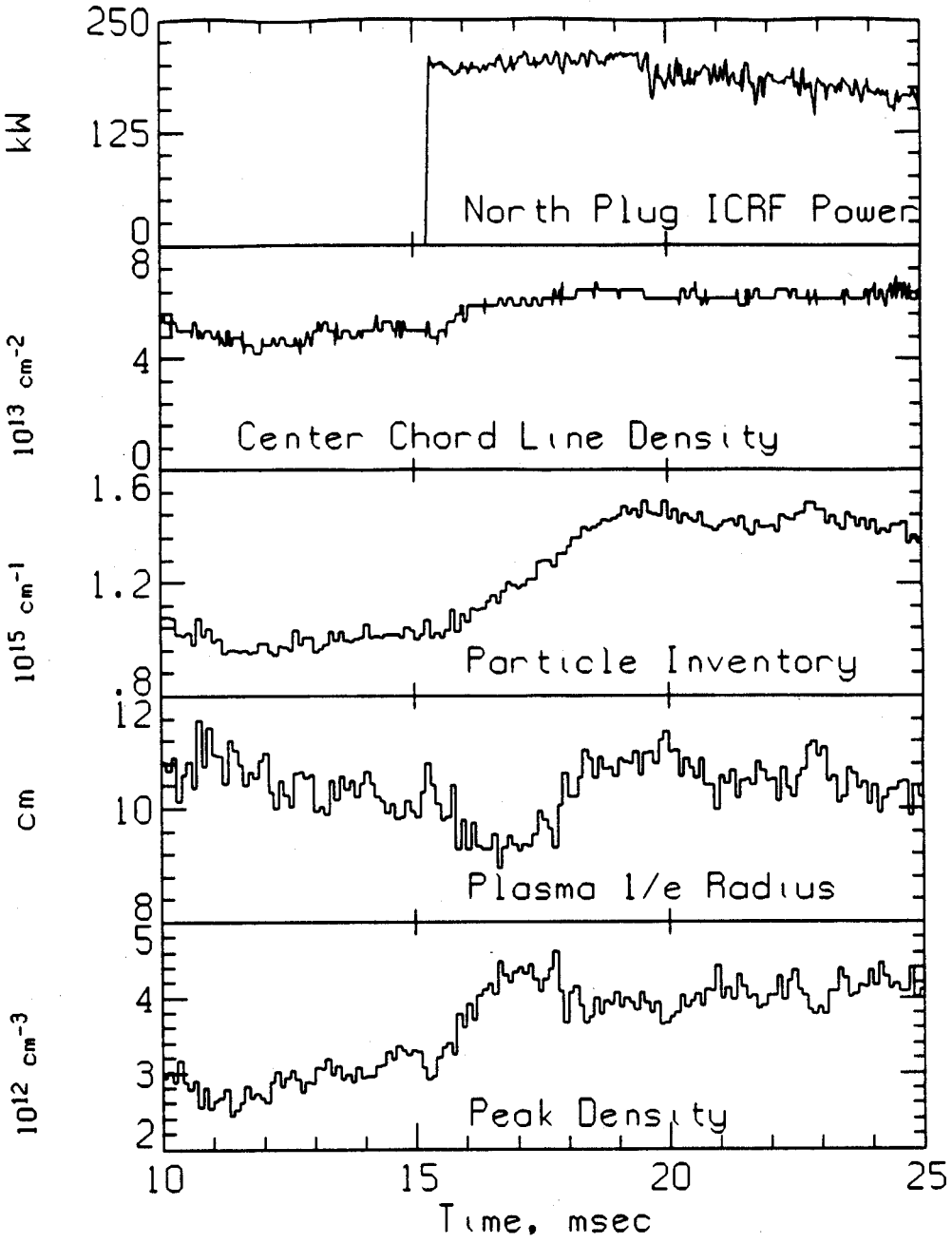

Figure 5. The particle inventory increases during application of ICRF (ion cyclotron range of frequencies) in one "plug" cell. The accounting of the particle inventory is not obvious from a line integrated density measurement however, since both the peak density and the $1/e$ radius are evolving together.

in the "plug" cell. After about 1.5 msec, the peak density saturates, but the profile radius increases for another 2.5 msec. The particle inventory, given by

$$N = L \int dA\, n(\mathbf{r}), \tag{12}$$

increases continuously during this time, corresponding to decreased axial losses of particles. The profile evolution is a key element in accountability of particles during plugging. This behaviour is not measurable by single chord line integral density measurements.

VI Conclusion

We have generated an algorithm for analysing two-dimensional density profiles from sparse one-dimensional interferometer arrays provided that the plasma profile is rigid, and that the parameters of the profile evolve over timescales longer than MHD rotation times. We have written an automated analysis program that runs unattended in "real-time" during Tara runs to provide processed density profile information.

The code for this analysis is written in FORTRAN on VAX architecture, and is available from one of the authors (JAC). We are pleased

to acknowledge the technical support of W. Brooks, W. Stein, and F. Yee. This work was supported by the Department of Energy under contract number DE-AC02-78ET51013.

References:

[1]N.R. Sauthoff, K.M. McGuire, and S. von Goeler. *IEEE Trans. Plasma Sci.* **PS-7,** 141 (1979)

[2]N.R. Sauthoff, K.M. McGuire, and S. von Goeler. *Rev. Sci. Instrum.* **57,** 2139 (1986)

[3]R. Nazikian and L.E. Sharp. *Rev. Sci. Instrum.* **58,** 2086 (1987)

[4]A.R. Jacobson. *Plasma Phys.* **23,** 927 (1981)

[5]A.R. Jacobson. *Plasma Phys.* **24,** 1111 (1982)

[6]J. Kesner, R.S. Post, B.D. McVey, and D.K. Smith. *Nucl. Fusion* **22,** 549 (1982)

[7]E. Sevillano, K. Brau, P. Goodrich, J. Irby, M. Mauel, R.S. Post, D.K. Smith, and J. Sullivan. *Rev. Sci. Instrum.* **56,** 960 (1985)

[8]W.H. Press, B.P. Flannery, S.A. Teukolsky, and W.T. Vetterling 1986, *Numerical Recipes* (Cambridge University Press), Chapter 14.

[9]M.N.Rosenbluth, N.A.Krall, N. Rostoker, Nucl Fusion Suppl., Pt. 1,143 (1962).

[10]M.N. Rosenbluth and A. Simon, Phys. Fl **8**, 1300 (1965).

[11]J.H. Irby, B.G. Lane, J.A. Casey, K. Brau, S.N. Golovato, W.C. Guss, S.F. Horne, J. Kesner, R.S. Post, E. Sevillano, J.D. Sullivan, and D.K. Smith. (Accepted for publication by *Phys. Fluids.*)

[12]J.A. Casey, B.G. Lane, J.H. Irby, K.L. Brau, S.N. Golovato, R.S. Post, and E. Sevillano. MIT report PFC/JA-87-25 (1987) *(Submitted to Phys. Fluids.)*